

## **Simulations of Dynamics and Transport During the September 2002 Antarctic Major Warming**

Gloria L. Manney,<sup>1,2</sup> Joseph L. Sabutis,<sup>3</sup> Douglas R. Allen,<sup>4</sup> William A. Lahoz,<sup>5</sup>  
Adam A. Scaife,<sup>6</sup> Cora E. Randall,<sup>7</sup> Steven Pawson,<sup>8,9</sup> Barbara Naujokat,<sup>10</sup> and  
Richard Swinbank<sup>6</sup>

Submitted to JAS Special Issue on SH 2002 Winter

---

<sup>1</sup>Jet Propulsion Laboratory, California Institute of Technology, Pasadena, California, USA.

<sup>2</sup>Department of Natural Sciences, New Mexico Highlands University, Las Vegas, New Mexico, USA.

<sup>3</sup>School of Education and Department of Mathematical Sciences, New Mexico Highlands University, Las Vegas, New Mexico, USA.

<sup>4</sup>Remote Sensing Division, Naval Research Laboratory, Washington, DC, USA.

<sup>5</sup>Data Assimilation Research Centre, Department of Meteorology, University of Reading, Reading, UK.

<sup>6</sup>Met Office, Bracknell, UK.

<sup>7</sup>Laboratory for Atmospheric and Space Physics, University of Colorado, Boulder, CO, USA.

<sup>8</sup>NASA/Goddard Space Flight Center, Greenbelt, MD.

<sup>9</sup>Goddard Earth Science and Technology Center, UMBC, Baltimore, MD

<sup>10</sup>Institut für Meteorologie, Freie Universität Berlin, Germany.

## Abstract

A mechanistic model simulation initialized on 14 September 2002, forced by 100 hPa geopotential heights from Met Office analyses, reproduced the dynamical features of the 2002 Antarctic major warming. The vortex split on  $\sim 25$  September, recovery after the warming, westward and equatorward tilting vortices, and strong baroclinic zones in temperature associated with a dipole pattern of upward and downward vertical velocities were all captured in the simulation. Model results and analyses show a pattern of strong upward wave propagation throughout the warming, with zonal wind deceleration throughout the stratosphere at high latitudes before the vortex split, continuing in the middle and upper stratosphere and spreading to lower latitudes after the split. 3D Eliassen-Palm fluxes show largest upward and poleward wave propagation in the  $0\text{--}90^\circ\text{E}$  sector prior to the vortex split (coincident with the location of strongest cyclogenesis at the model's lower boundary), with an additional region of strong upward propagation developing near  $180\text{--}270^\circ\text{E}$ . These characteristics are similar to those of Arctic wave 2 major warmings, except that during this warming, the vortex did not split below  $\sim 600$  K. The effects of poleward transport and mixing dominate modeled trace-gas evolution through most of the mid-to-high latitude stratosphere, with a core region in the lower stratospheric vortex where enhanced descent dominates and the vortex remains isolated. Strongly tilted vortices led to low-latitude air overlying vortex air, resulting in highly unusual trace gas profiles. Simulations driven with several meteorological datasets reproduced the major warming, but in others stronger latitudinal gradients at high latitudes at the model boundary resulted in simulations without a complete vortex split in the midstratosphere. Numerous tests indicate very high sensitivity to the boundary fields, especially the wave 2 amplitude. Major warmings occurred for initial fields with stronger winds and larger vortices, but not smaller vortices, consistent with the initiation of wind deceleration by upward propagating waves near the poleward edge of the region where wave 2 can propagate above the jet core. Thus, given the observed 100 hPa boundary forcing, stratospheric pre-conditioning is not needed to reproduce a major warming similar to that observed. The anomalously strong forcing in the lower stratosphere can be viewed as the primary direct cause of the major warming.

## 1. Introduction

Stratospheric major warmings (wherein the usually strong westerlies of the polar night jet are reversed to easterlies and high latitude temperature gradients reverse) are the most dramatic events affecting the wintertime circulation and transport in the northern hemisphere (NH). Historically, such warmings have occurred in approximately half of NH winters (e.g., Labitzke, 1977, 1982; Naujokat et al., 2002), except during the unusually cold period in the 1989-1990 through 1997-1998 winters (Manney et al., 1999). Because of the typically much lower temperatures and stronger polar vortex in the southern hemisphere (SH), the occurrence of the first observed major warming in the Antarctic in mid-late September 2002 (e.g., Varotsos, 2002; Baldwin et al., 2003; Allen et al., 2003; Weber et al., 2003) was completely unanticipated. As shown by, e.g., Allen et al. (2003), Newman and Nash (this issue), and Scaife et al. (this issue), the 2002 SH winter stratosphere was unusually disturbed beginning in May. Several minor warmings occurred in August and September, culminating in a major warming beginning in mid-September that strongly resembled what are commonly referred to as “wave-2” warmings (in which the midstratospheric polar vortex splits) in the NH (e.g., Allen et al., 2003). The major warming was immediately preceded by an extraordinarily strong (much stronger than typically observed during NH major warmings) pulse of eddy heat flux in the lower stratosphere/upper troposphere, indicating unusual upward planetary-scale wave propagation (e.g., Allen et al., 2003; Sinnhuber et al., 2003, Newman and Nash, this issue; Scaife et al., this issue).

Mechanistic model simulations have been instrumental in helping to understand the dynamics of stratospheric sudden warmings. Butchart et al. (1982) were among the first to use a detailed primitive equation model to test sensitivity of simulations to realistic initial and boundary conditions. Smith (1992) used a mechanistic model to explore sensitivity of major warming occurrence to initial and boundary fields from various times. Manney et al. (1994a) compared simulations of the February 1979 major warming using isentropic and pressure coordinate models, and examined sensitivity to initial date, forcing datasets, radiation scheme and model resolution. Jung et al. (2001) used an isentropic vertical coordinate model and boundary sensitivity tests to examine the role of various mechanisms in the recovery phase of the February 1979 major warming. These studies helped elucidate characteristics of boundary and initial conditions important to simulating major warmings, and hence shed light on the mechanisms involved

in producing such warmings. Simulations of major warmings have also been used to study development of small-scale structure (e.g., Fairlie et al., 1990a; Manney et al., 1994a) and details of air motion and tracer transport (e.g., Manney et al., 1994a, 2000a), topics for which observation-based datasets are often too incomplete, sparse, or of too coarse resolution to study in detail.

Several studies have used more idealized simulations to examine aspects of the NH stratospheric circulation and the conditions under which major warmings occur. O'Neill and Pope (1988) used mechanistic model simulations to contrast the response of the stratosphere to weak and strong boundary level forcing, showing the importance of nonlinear effects in the strong forcing regimes under which major warmings may occur, and arguing against the relevance of the “pre-conditioning” concept as applied to the occurrence of major warmings. Scott and Haynes (1998) showed that interannual variability, including stratospheric warmings, arose from internal variability under certain ranges of boundary forcing, and argued that zonal flow anomalies in the subtropics were responsible for this variability. Scaife and James (2000) showed weak, moderate and strong forcing regimes in the NH winter, leading to strong westerly flow, unsteady westerly flow, and oscillations between westerly and easterly flow, respectively. Gray et al. (2003) used a mechanistic model with an ensemble approach to investigate the response of the NH stratospheric flow regime to changes in tropospheric wave forcing and equatorial wind direction. They found that major warmings always occurred with strong forcing and never occurred with weak forcing, but in an intermediate forcing regime, tropospheric forcing was less critical and other factors such as early-winter initial conditions and the quasi-biennial oscillation (QBO) phase influenced the occurrence of major warmings.

Here we have used the UK Universities Global Atmospheric Modelling Project (UGAMP) Stratosphere-Mesosphere Model (USMM) to simulate the SH 2002 stratospheric major warming. Having obtained a very realistic simulation of the event, we use the observations and simulations to examine aspects of the dynamics of the warming, and modeled long-lived tracers to give an overview of transport. Sensitivity tests to changes in initialization and boundary forcing are used to elucidate some of the important features of the stratospheric flow conditions that allowed this unprecedented warming to occur.

## 2. Model and Data Description

### *a. USMM model description*

The USMM (Thuburn and Brugge, 1994) is a spectral, primitive equation model of the stratosphere and mesosphere forced at the lower boundary by specified geopotential height fields. The configuration of the USMM used here is the same as that described by Manney et al. (2002). This configuration has 34 isobaric levels from 89.5 to 0.01 hPa (MacKenzie et al., 1999) (vertical resolution  $\sim 1.6$  km), a lower boundary at 100 hPa, an upper boundary condition of no mass flux through zero pressure, and a truncation at T42 (horizontal resolution  $\sim 3^\circ$ ). The model has extra scale-selective diffusion in the mesosphere, which, with the short radiative time scales there, helps to damp waves and reduce the possibility of wave reflection at the boundary.

Gravity-wave drag is parameterized by applying a simple Rayleigh friction with an altitude dependent damping coefficient (damping times range from 116 d at and below 50 km to 1.4 d at 80 km) to the zonal wind (Thuburn and Brugge, 1994; MacKenzie et al., 1999). While the USMM can be run with a non-orographic gravity-wave scheme, the selection of gravity wave characteristics is problematic and largely arbitrary (e.g., Manney et al., 2002), and the model has previously been used successfully to simulate major warmings without including this scheme (Manney et al., 1999).

The USMM uses the MIDRAD radiation scheme (Shine, 1987), with seasonally and meridionally varying upwelling fluxes of IR radiation in the  $9.6 \mu\text{m}$  and  $15 \mu\text{m}$  wavelength regions calculated using climatological temperatures assuming that emission at  $9.6 \mu\text{m}$  originates at 700 hPa and emission at  $15 \mu\text{m}$  originates at 130 hPa. A prescribed, zonal mean climatological ozone field is used in the radiation calculations. The USMM's online transport calculation is described by Thuburn and Brugge (1994); a standard spectral scheme is used in the horizontal, with a flux-limited scheme in the vertical.

### *b. Initialization and boundary fields*

For most of the results shown here, the model was forced at 100 hPa using daily geopotential heights from the UK Met Office's stratosphere-troposphere assimilation system (Swinbank and O'Neill, 1994; Swinbank et al., 2002) and initialized using Met Office three-dimensional (3D) wind and temperature fields. Met Office winds and temperatures above their top level of

0.3 hPa are extrapolated up to the top USMM level using thermal wind balance in the zonal mean. Sensitivity tests to initialization date and configuration of initial and boundary fields are all done using the Met Office data. The sensitivity of the model simulations to the dataset used for initialization and forcing is tested in simulations using data from the US National Centers for Environmental Prediction (NCEP)/Climate Prediction Center (CPC), the European Centre for Medium-Range Weather Forecasts (ECMWF), and NASA's Goddard Earth Observation System (GEOS) version 3 (GEOS-3) and version 4 (GEOS-4) assimilation systems. These comprise the most commonly used gridded meteorological datasets that cover the stratosphere. Except for GEOS-4, the main features of these datasets are described by Manney et al. (2003). The high resolution GEOS and ECMWF data have been interpolated to  $2 \times 2.5^\circ$  and  $2.5 \times 2.5^\circ$  grids, respectively. The ECMWF data are from the operational assimilations for SH 2002 (see Simmons et al., this issue). The GEOS-4 data use the Physical Space Statistical Analysis Scheme (Cohn et al., 1998), as in GEOS-3, but with a new model (Lin, 2004); see Schoeberl et al. (2003) and Douglass et al. (2003) for further details.

Four chemical tracers and several idealized tracers were included in the model simulations. Idealized tracers are initialized with potential vorticity (PV), latitude,  $\log_{10}(\text{pressure})$ ,  $\log(\text{potential temperature } (\theta))$ , and equivalent latitude (EqL, the latitude equivalent to the area enclosed by each PV contour; similar to the "tracer equivalent latitude" used by Allen et al. (2003), and references therein, with small vertical gradients, so it emphasizes horizontal motions). Methane ( $\text{CH}_4$ ), water vapor ( $\text{H}_2\text{O}$ ), nitrous oxide ( $\text{N}_2\text{O}$ ), and ozone are initialized with 3D fields reconstructed from EqL/ $\theta$ -space mappings of Upper Atmosphere Research Satellite (UARS) long-lived trace gas data from a "climatology" based on Cryogenic Limb Array Etalon Spectrometer  $\text{CH}_4$  and  $\text{N}_2\text{O}$ , and Microwave Limb Sounder  $\text{H}_2\text{O}$  and ozone, from April 1992 through March 1993 (e.g., Manney et al., 2000b). The UARS  $\text{CH}_4$ ,  $\text{N}_2\text{O}$ , and  $\text{H}_2\text{O}$  fields used here are not reliable below 68 hPa (or in some cases lower pressure in low latitudes), so the initialization fields contain some artifacts which can produce unrealistic results in the lowest levels. The idealized tracers that isolate vertical motion (the  $\log(\theta)$  and  $\log_{10}(\text{pressure})$  tracers) show clearly that the model's vertical transport is not realistic in the lowest levels; thus, quantitative estimates of diabatic descent from the tracer fields are not attempted below  $\sim 550$  K.

The control simulation was initialized on 14 September 2002 and forced using Met Office 100 hPa geopotential heights. This initialization date was chosen as one with a lull in wave

activity at 100 hPa prior to the development of the warming. Other simulations test the sensitivity to initialization date, initial fields and boundary forcing. Boundary fields are provided to the model once-daily at 12UT. For sensitivity tests in which the boundary or initial fields are altered so that they may be dynamically inconsistent, the boundary fields are relaxed from the initial day's 100 hPa geopotential heights to the desired value over the first three days.

PV (and horizontal winds from the NCEP/CPC analyses) is calculated from the meteorological analyses (Newman et al., 1989; Manney et al., 1996) for comparison with PV from the USMM simulations, which is an output of the USMM's postprocessing program and is thus calculated using a different algorithm; there is therefore sometimes a bias between the two fields. Eliassen-Palm (EP) fluxes (e.g., Andrews et al., 1987, and references therein) and indices of refraction (e.g., Matsuno, 1970), which provide measures of wave propagation, and 3D EP fluxes (Plumb, 1985) are calculated as described by Sabutis (1997) and Sabutis et al. (1997), respectively.

### **3. Modeling Dynamical Evolution During the SH 2002 Major Warming**

#### *a. Synoptic Evolution*

Our first simulation of the SH 2002 major warming was initialized on 14 September 2002. This initialization date was chosen during a relative minimum in wave 2 activity at 100 hPa, the model's lower boundary. Figure 1 shows the boundary field (Met Office 100 hPa geopotential heights) in the days leading up to the vortex split. There is strong and persistent cyclogenesis (trough formation) in the 0–90°E sector, and weaker and more sporadic cyclogenesis near 270°E; this is manifested in a wavenumber decomposition as a large amplification of wave 2 in the boundary forcing. The stronger anticyclone in the midstratosphere forms downstream of the region of strongest cyclogenesis, near 120°E, beginning around 20 September and culminating in a vortex split in the midstratosphere around 25 September. Fairlie and O'Neill (1988) and Fairlie et al. (1990b) saw similar behavior during “wave 2” warmings in the NH, and argued that the development of the anticyclone was associated with that cyclogenesis.

Figure 2 shows 10 hPa zonal mean wind, zonal mean temperature, and wave 1 and wave 2 in geopotential height for the 37-day simulation period from the Met Office analyses and the USMM simulation; Figure 3 shows a vertical section at 60°S of the same quantities. These figures show a

remarkably faithful simulation of the analyzed flow. The largest difference is a slightly slower and weaker recovery of the 10 hPa zonal mean winds after the warming in the USMM. In the upper stratosphere, however, the modeled westerly winds recover slightly faster than in the analysis. Zonal mean winds reverse first near the pole in the upper stratosphere, with the time of the wind reversal near 60°S corresponding to the time of the vortex split. The latitudinal extent of reversed temperature gradients echos that of the wind reversal, with a downward progression of warming seen in Figure 3. At the peak of the warming, wave 2 amplitude is at a maximum in the middle and upper stratosphere, with the earlier peak of wave 2 near the boundary clearly apparent in Figure 3. Throughout the warming period, wave 1 and wave 2 amplitudes are anti-correlated in time.

Maps of sPV (PV scaled in “vorticity units”, e.g., Dunkerton and Delisi, 1986; Manney et al., 1994b) on the 840 K isentropic surface during the warming (Figure 4) show a “wave-2” type major warming in which the vortex splits in the midstratosphere (25 September) and one fragment then moves into low latitude and dissipates, while the other moves back over the pole (e.g., 1 October) and eventually strengthens. These maps show the modeled morphology and evolution of PV and temperature closely following the analyses. Consistent with the zonal means shown in Figure 2, the modeled vortex at 840 K upon recovery is smaller and weaker, and temperatures slightly higher, than in the analyses. Many previous simulations of stratospheric major warmings using pressure-coordinate mechanistic models have failed to reproduce complete recovery of the westerly flow and realistic strengthening of the vortex after otherwise successful simulations (e.g., Manney et al., 1994a, 1999). A USMM simulation of the February 1989 wave 2 major warming (not shown), though reproducing the vortex-split well, also shows a more substantial delay in recovery after the warming than our simulation of the SH major warming. This may be because, as confirmed by examination of several cases, the wave activity after the SH warming is weaker than after typical NH warmings, so the SH recovery was more radiatively controlled.

A qualitative view of the 3D evolution of the vortex during the simulation is given in Figure 5, showing an isosurface of sPV throughout the stratosphere. An animation of these isosurfaces for the entire simulation is given in the supplemental electronic material. As the vortex splits in the upper and middle stratosphere, both vortices tilt westward and equatorward with height. The vortex initially in the 180–270°E sector shows a stronger westward tilt, as it is drawn out into a long ribbon into mid latitudes and back over the pole at the highest levels. This vortex eventually breaks up, while the other moves back over the pole, becomes upright, and eventually strengthens.

The westward and equatorward tilt with height is typical of NH major warmings (e.g., Fairlie et al., 1990a; Manney et al., 1994a, 1999), but unlike many NH warmings (e.g., Manney et al., 1994a, Krüger et al., this issue), the vortex does not fully split in the lower stratosphere, but only down to  $\sim 600$  K (see Allen et al., 2003, Kondragunta et al., this issue). The stripping off and rolling up of vortex material beginning in the upper stratosphere and extending down through the mid-stratosphere is very similar to behavior shown by Manney et al. (1994a, 1999) for NH major warmings, and also strongly reminiscent of the idealized simulations shown by Polvani and Saravanan (2000). Aspects of the behavior seen here resemble Polvani and Saravanan's experiment with large wave 2 amplitude forcing, and with wave 1 forcing of an initially vertically sheared jet; these cases shown by Polvani and Saravanan are ones in which the initial vortex structure allows waves to propagate into the upper stratosphere before beginning to break. Polvani and Saravanan suggest that this may lead to stronger warmings because wave breaking begins at higher, rather than lower, levels.

Temperature and vertical velocity (six-hour averages centered at 12UT in the Met Office data, at 12UT in the USMM) cross-sections (Figure 6) show that baroclinic zones (regions of extremely strong, tilting, temperature gradients resembling upper tropospheric fronts) appear during the warming, forming as the warming begins and strengthening until the vortex splits, similar to those in simulations of NH major warmings (e.g., Fairlie et al., 1990a; Manney et al., 1994a, 1999). The pattern of vertical velocities, with downward motion over and to the east and weak upward motion below and to the west of the baroclinic zone, acts to strengthen the temperature gradients. Horizontal maps (not shown) indicate a dipole pattern of upward and downward motion across the vortex edge as shown by Manney et al. (1994a) for the NH. The narrow bands of alternating upward and downward vertical velocities extending eastward and upward above the eastern baroclinic zone strongly resemble features described by Fairlie et al. (1990a) that they showed to be consistent with inertio-gravity waves generated along the baroclinic zone. The maximum vertical and horizontal temperature gradients ( $\sim 10$  K/km and  $\sim 27$  K/1000km, respectively) are slightly larger than those reported by Fairlie et al. (1990a) and Manney et al. (1994a) for NH simulations.

Earlier studies (e.g., Manney et al., 1994a; Fairlie et al., 1990a) of NH warmings typically used NCEP/CPC objective analyses, other analyses based on TIROS Operational Vertical Sounder data, or simple analyses of Limb Infrared Monitor of the Stratosphere satellite temperature data

to compare with simulations, as opposed to the analyses used here that are based on assimilation models using a comprehensive general circulation model (GCM). While the data ingested are similar, the use of a GCM in the assimilation process can refine small-scale structure such as baroclinic zones that would not be well-resolved in simpler analyses of coarse resolution data. The Met Office analyses show horizontal and vertical temperature gradients comparable to those generated in the USMM, in contrast to earlier comparisons where the analyses used did not fully resolve baroclinic zones. Simmons et al. (this issue) also demonstrate the ability of the ECMWF assimilation products to capture small-scale structure. The USMM, however, provides a more realistic representation of the temperature structure near the stratopause, where the Met Office assimilation system is at a disadvantage in being near the top of the analysis system and where the data ingested are increasingly sparse and uncertain.

*b. Diagnostics of Wave Propagation and Interactions*

EP fluxes serve as indicators of wave propagation and wave-mean flow interactions. Figure 7 shows cross-sections of EP flux and divergence from the analyses and the USMM leading up to and after the vortex split. Strong upward propagation and some zonal wind deceleration throughout the high-latitude stratosphere begins on  $\sim$ 20 September and by 22 September upward propagation intensifies, with fluxes directed poleward in the lower to middle stratosphere. Zonal wind deceleration intensifies through 26 September, with maximum deceleration moving to lower latitudes in a progressively broader region as upward propagating waves are steered equatorward. After 26 September, wave propagation is directed equatorward in the lower stratosphere and acceleration of the zonal mean winds begins in the upper stratosphere. Examination of the indices of refraction for waves 1 and 2 (not shown) indicates a broad corridor for upward and poleward propagation throughout the stratosphere for both waves (narrower on the poleward side for wave 2) prior to the warming, with maximum deceleration beginning along the poleward boundary in the upper stratosphere; the region narrows on the poleward side, and cuts off in the mid-stratosphere as the winds reverse. This is consistent with the poleward direction of the fluxes on 22 September and the equatorward tilt and broader, but lower altitude, region of deceleration seen on 26 September.

The longitudinal distribution of propagation is shown in the 3D EP fluxes (Figure 8). The patterns of 3D EP flux in the USMM and analyses are in very good agreement. Strongest upward

propagation in the lower stratosphere leading to the major warming seen in Figure 7 is seen to originate primarily from the 0–90°E sector prior to the vortex split (3D EP fluxes for levels down through 100 hPa show very similar patterns, and large values on earlier days are confined entirely to the 0–90°E sector), coincident with the region of strongest cyclogenesis in the boundary fields shown in Figure 1, with a secondary maximum appearing in the 180–270°E sector after 22 September. The regions of strong upward propagation are associated with downward air parcel motion and warming (e.g., Sabutis et al., 1997); temperatures increase in these regions (e.g., Figure 8, 26 September) and the centers of strongest upward propagation are approximately coincident with the large downward vertical velocities seen in Figure 6, lying across the boundary between the vortex and the anticyclone. The horizontal 3D EP flux vectors in Figure 8 show that the strong wave activity in the 0–90°E sector is primarily poleward before the vortex splits. While there is still significant poleward wave activity in that sector on 26 September (as well as some equatorward motion at the eastern edge of it), there is more equatorward wave motion in the 180–270°E, resulting in the equatorward tilt of the 2D EP fluxes on that day (Figure 7) in the lower stratosphere.

The apparent anti-correlation between wave 1 and wave 2 amplitudes seen in Figures 2 and 3 suggests that non-linear wave-wave interactions may be occurring during the warming. In agreement with O’Neill and Pope (1988) and Fairlie and O’Neill (1988), calculations for both the USMM and analyses indicate that non-linear interactions are of comparable magnitude to perturbation/mean-flow interactions.

### *c. Modeled Transport*

The dynamical evolution discussed above results in highly unusual patterns of transport during the warming. Cross-sections of USMM CH<sub>4</sub> and EqL-tracer (Figure 9) show the vortex edge clearly defined in the tracer fields, with very low CH<sub>4</sub> values inside the vortex and strong gradients at the vortex edge; H<sub>2</sub>O and N<sub>2</sub>O are not shown, but their behavior exhibits similar features to those in CH<sub>4</sub>. The elevated contours (higher CH<sub>4</sub>) outside the vortex indicate low-latitude air drawn into this region, as demonstrated from the EqL-tracer. The contours with largest upward excursions are coincident with upward vertical velocities (Figure 6) and locally downward wave propagation (Figure 8). On 26 September, the large separation and strong westward tilt of both vortices in the middle stratosphere are apparent in the CH<sub>4</sub> fields.

By 28 September both vortices have limited vertical extent with higher  $\text{CH}_4$  values typical of mid-to-low latitudes above them; the EqL-tracer clearly shows that low-latitude air surrounds the vortices above and on both sides. The strong tilt of the vortices with height thus results in very unusual vertical tracer gradients. Hoppel et al. (2003), Allen et al. (2003) and Kondragunta et al. (this issue) discuss some of the effects of this strong tilt on observed ozone distributions, and Randall et al. (this issue) detail the effects on ozone from solar occultation observations compared with that passively transported in the USMM. The lowest  $\text{CH}_4$  values seen in the polar vortex near 22 hPa during the warming were confined above  $\sim 5$  hPa inside the vortex prior to the warming, confirming very strong descent in the vortex region during the warming. Examination of the  $\log(\theta)$ -tracer indicates descent rates of  $\sim 10$  K/day ( $d\theta/dt$ ) in the middle stratosphere (800-1100 K) between 14 and 28 September in the western vortex, and localized descent up to  $\sim 6$  K/day just outside it.

Despite the enhanced descent, the overall tracer evolution between 14 September and 6 October 2002 (Figure 10) indicates that poleward transport and mixing are dominant throughout mid-to-high latitudes above  $\sim 800$  K. In the lower stratosphere, a region is apparent in the vortex core where descent dominates. Examination of the PV and  $\log(\theta)$ -tracers shows net descent rates over the period shown of  $\sim 6.5$  K/day, 10 K/day, and 3 K/d in the upper, middle and lower stratosphere, respectively, comparable to previous estimates for NH warmings (e.g., Manney et al., 1994a). The overall picture of large-scale transport during the warming shows both enhanced descent in the vortices and anticyclones, and greatly enhanced poleward transport/mixing over that seen in a typical SH winter. In determining long-lived tracer evolution, isentropic poleward transport and mixing dominate except in the core of the lower stratospheric vortex (below  $\sim 750$  K and poleward of  $\sim -80^\circ$ EqL). Randall et al. (this issue) explore in detail the transport reflected in “proxy” ozone derived from POAM III, HALOE and SAGE III data, and compare this with the ozone passively transported in the USMM.

#### **4. Sensitivity Tests and Dynamical Implications**

##### *a. Simulations Driven by Different Meteorological Analyses*

Stratospheric transport studies are sensitive to the meteorological datasets used (e.g., Manney et al., 2003). To investigate this sensitivity in the USMM simulations, we have done simulations

from 14 September driving the model with ECMWF, NCEP/CPC and GEOS-3/GEOS-4 fields. Figure 11 shows 10 hPa zonal mean zonal winds from each of these analyses and the corresponding USMM simulations. While the ECMWF and NCEP/CPC driven simulations reproduce the warming as well as the control run (driven with Met Office data), runs driven with GEOS-3 and GEOS-4 show wind reversals in smaller regions poleward of  $\sim 70^\circ\text{S}$  and equatorward of  $\sim 50^\circ\text{S}$ . The GEOS driven simulations appear very faithful through  $\sim 22$  September, but fail to capture the complete splitting of the vortex (e.g., Figure 12; a complete split being defined as when the strong PV gradient regions form two *separate* closed curves).

Simulations using Met Office fields for initialization and GEOS-4 for the lower boundary also failed to produce the split vortex; conversely, when GEOS-4 was used for initialization but Met Office for the boundary, a major warming was simulated. Examination of the vertical EP flux from the simulations (not shown) at 100 hPa indicates significant differences: the GEOS fields show a decrease, shortly before the vortex splits, in strong upward wave 2 propagation. This large difference is not apparent in the 100 hPa EP fluxes calculated from the analyses, indicating that the small differences in the input boundary fields are affecting the lowest levels of the model so as to make the fields less favorable for upward propagation.

Examination of the 100 hPa geopotential heights used as boundary forcing does not reveal obvious differences in wave characteristics that stand out in GEOS versus the other analyses. However, the GEOS zonal mean 100 hPa geopotential heights have noticeably larger latitudinal gradients and lower values near the pole. A simulation initialized with Met Office data, using the GEOS-4 zonal mean and Met Office wave components in the boundary field, did not completely split the vortex. A simulation initialized with GEOS-4 data, using the Met Office zonal mean and GEOS-4 wave components did split the vortex. A simulation driven with GEOS-4 data, but with the 100 hPa zonal mean heights increased at all latitudes by 0.4% (to give values near the pole as large as those in the Met Office data but with the same latitudinal gradients as in the GEOS-4 data) did not produce a major warming. The difference in the 100 hPa zonal mean heights and latitudinal gradients thus appears to be a major factor in the failure of the GEOS-driven simulations to reproduce the observed vortex evolution. The sensitivity to these small differences suggests very strong dependence of warming characteristics on details of the lower boundary forcing.

### *b. Sensitivity to Initialization and Boundary Forcing*

Previous studies have altered the initialization and/or boundary fields in mechanistic models to examine characteristics important for simulating major warmings. Butchart et al. (1982) varied initial states and wave 2 characteristics in the boundary field to examine the sensitivity of simulations of the February 1979 major warming. Smith (1992) combined initial and boundary fields from different times to examine the role of preconditioning in the occurrence of major warmings. Here, sensitivity tests varying the Met Office fields used for initialization and boundary forcing (described below and summarized in Table 1) help us to understand what characteristics of the driving fields are important in simulating the SH major warming. The results show strong sensitivity to boundary forcing and to some characteristics of the initialization fields.

When only waves 1 and 2 are included in the boundary field, the vortex does not completely split and there is no wind reversal near 60°S (Figure 13); with waves 1–3 or waves 2–3 in the boundary field, the warming strongly resembles that observed (Figure 13). When the 100 hPa wave 1 is excluded, the wave 2 amplitude at 10 hPa grows nearly monotonically until ~25 September and decays smoothly thereafter, and winds recover more slowly and weakly near the pole (Figure 13). This supports the idea that the vacillation in wave 2 amplitudes seen in the control run may arise from non-linear interactions between wave 1 and wave 2; it also indicates that the vacillation is not needed for the major warming to occur, but does play a significant role in the recovery, similar to the results of Jung et al. (2001) for the NH February 1979 warming. In runs with altered wave 2 phases (Figure 14), a major warming occurs, but is more dominated by wave 1 (Figure 15) and the vortex does not split until 30 September–2 October. No runs with decreased boundary wave amplitudes resulted in strong warmings.

Figure 16 shows the 14 September zonal mean winds for the control run, runs initialized with 14 September 1997 and 14 September 2001 fields, and the run initialized on 27 July 2002. These cases represent substantial differences in the strength and structure of the jet, which affects wave propagation. On 14 September 2002, the jet is weak and the vortex relatively small (i.e., the jet core is at high latitude); in 1997, the vortex is even smaller but the jet is stronger; in 2001, the vortex is both large and strong. The runs with earlier initializations (the 27 July initialization, Figure 16, is the extreme case) evolve so that, by 14 September, the vortex is smaller but stronger than that observed.

The run with the 2001 (large, strong vortex) initialization produces a wave 2 major warming that becomes stronger than that in the control run (Figures 17 and 18). The run with the 1997 initialization produces a very strong, but not major, warming (Figure 17) where the vortex nearly splits on 26 September (Figure 18), but then begins to recover. Runs with a zonally symmetric initial state based on 14 September 2002 (Figure 17) and with the zonal mean wind component enhanced in a 14 September 2002-based initial state also produce major warmings. The vortex split in the run initialized on 11 September 2002, but the two vortices were not as widely separated as in the control run, resulting in winds remaining westerly in a small region poleward of  $60^{\circ}\text{S}$ ; runs with progressively earlier initializations (29 and 11 August, and 27 July) produced simulations without a vortex split, with increasingly weaker (though still very strong by SH standards) wave 1-dominated warmings. Thus, the cumulative effect of small discrepancies developing in the model alters the jet structure to be less favorable to the wave propagation resulting in the warming.

Examination of wave activity and refractive indices (Figure 16 also shows the wave 2 refractive index) indicates that, for smaller vortices, the region where wave 2 propagates through the middle and upper stratosphere (above  $\sim 15$  hPa) extends further poleward, thus focusing the wave propagation to the region of the jet core; zonal mean wind deceleration occurs at and below the jet core, but not above it. In contrast, for 14 September 2001 and 14 September 2002, the waves propagate above the jet core, leading to deceleration both above and below the jet core (e.g., Figure 7), and a stronger, more prolonged, warming. That stronger warmings occur when waves can initially propagate higher is consistent with the 3D vortex evolution shown in Figure 5 and the animation indicating wave-breaking (stripping of vortex material) beginning in the upper stratosphere, and similar to the idealized results of Polvani and Saravanan (2000). Analogous to the very strong warming resulting from the 14 September 2001 initialization, Polvani and Saravanan also show that stronger vortices can lead to stronger warmings because they may initially allow waves to propagate higher. Conversely, 3D plots similar to Figure 5 for the 27 July 2002 initialization (not shown) indicate vortex erosion beginning at lower levels, possibly shielding the upper stratosphere from upward propagating waves as suggested by Polvani and Saravanan (2000).

Significant differences in low latitude easterlies are also apparent in the initial fields (e.g., Figure 16), and those cases with stronger easterlies result in stronger warmings. All of the cases

discussed here show a poleward tilt of the upward propagating EP flux vectors before the warming, and increased poleward focusing of the waves in the cases with stronger easterlies is not readily apparent; however, it is possible that a subtle increase in poleward focusing related to stronger easterlies may play a minor role in determining the strength of the warmings. Consistent with this small effect, Gray et al. (this issue) show simulations suggesting that anomalously strong upper stratospheric equatorial easterlies in 2002 may play a role in the development of the warming but are unlikely to be its primary cause.

The production of a major warming with the 14 September 2001 initialization field demonstrates that “pre-conditioning” (e.g., Kanzawa, 1980; McIntyre and Palmer, 1983) in the conventional sense of having a smaller and/or weaker vortex before the warming is not essential for a major warming similar to that attributed to the anomalous tropospheric forcing in 2002 to occur; to the contrary, a smaller vortex can inhibit a major warming at this time. This is, at first glance, somewhat surprising since the warming followed a winter in which unusually strong, persistent wave activity led to an especially small, weak jet prior to the major warming (e.g., Allen et al., 2003, Newman and Nash, this issue; Scaife et al., this issue). The vortex can certainly be considered pre-conditioned in September 2002; what our tests demonstrate is that, given the observed forcing at 100 hPa, this stratospheric pre-conditioning is not a necessary condition for a major warming to occur. There is, indeed, sensitivity to the initial state in the stratosphere (also apparent in GCM simulations mentioned by Charlton et al., this issue), but this sensitivity does not conform to the conventional idea of “pre-conditioning.”

The high sensitivity of the model results to details of the boundary forcing, especially any diminution of wave 2 amplitude, suggests that the situation is analogous to the “strong forcing regime” of Scaife and James (2000) and Gray et al. (2003), where a major warming always occurs for a given boundary forcing. This would be consistent with the unprecedented strength (even compared to NH major warmings) of the wave fluxes observed preceding the SH 2002 major warming (e.g., Allen et al., 2003; Sinnhuber et al., 2003, Newman and Nash, this issue). However, with this huge wave event in the upper troposphere and lower stratosphere following a winter with uncharacteristically large wave activity in the stratosphere, the unusual wave forcing is unlikely to have occurred independently of the small, weak vortex prior to the warming. Scaife et al. (this issue) show that a wave pulse of modest amplitude lower in the troposphere was able to propagate unusually effectively into the lower stratosphere (e.g., to 100 hPa, where the USMM is

forced) because of a “pre-conditioned” vortex, and hence grow to extraordinary size in the upper troposphere and lower stratosphere. Thus, the unusual wave forcing and small, weak stratospheric vortex preceding the major warming cannot be regarded as being independent of each other, and the vortex structure, at least at lower levels, was instrumental in allowing formation of the wave pulse that directly triggered the warming.

## 5. Summary and Conclusions

A 3D primitive equation mechanistic model of the stratosphere and mesosphere has been used to simulate the Antarctic stratospheric major warming in September 2002. The control simulation was initialized on 14 September 2002 (about 13 days before the vortex split in the mid-stratosphere), driven with Met Office fields, and run through 20 October (well after the recovery). This simulation was remarkably successful at reproducing the dynamical features of the SH 2002 major warming, including the recovery phase, which many simulations of NH major warmings have not captured well. The excellent simulation of the warming itself suggests that the evolution of the stratospheric flow is largely determined by the 100 hPa geopotential heights that are prescribed in the model. Good simulation of the recovery may be linked to a recovery period where radiative effects are more dominant than for NH warmings. The simulation accurately showed the main features of the SH 2002 major warming:

- The vortices tilt westward and equatorward with height. Both vortices eventually disperse in the upper stratosphere and one reforms from below during the recovery. In contrast to NH wave 2 warmings, the vortex does not split in the lower stratosphere, below  $\sim 600$  K. This is likely related to the stronger SH lower stratospheric vortex before the warming.
- Strong baroclinic zones form along the edges of the vortices before and during the warming, resembling in many respects upper tropospheric fronts, with upward vertical velocities below and to the west and downward velocities above and to the east acting to strengthen the temperature gradients.
- EP fluxes show strong upward propagation in the lower stratosphere throughout the warming. The vectors initially tilt poleward and strong decelerations of the zonal wind throughout the stratosphere begin at very high latitudes. After the vortex splits the vectors turn equatorward, with strong deceleration continuing in the middle and upper stratosphere.

- 3D EP fluxes show the largest upward and poleward wave propagation in the 0–90°E sector before the vortex splits, coincident with the region of strongest cyclogenesis at 100 hPa.

These characteristics are overall very similar to those during NH wave 2 warmings. Krüger et al. (this issue) provide a detailed comparison of the SH major warming with the February 1989 “wave 2” major warming in the NH.

An overview of modeled large-scale transport during the warming shows enhanced diabatic descent in both the vortex and anticyclone regions, consistent with previous studies of NH major warmings (e.g., Manney et al., 1994a). In mid-to-high latitudes, however, enhanced poleward transport and mixing dominate the changes in trace gas distributions. The exception is in the core of the lower stratospheric vortex below  $\sim 700$  K, where changes are due primarily to enhanced descent, consistent with the observed behavior of ozone in the lower stratospheric vortex (Hoppel et al., 2003). This core region is somewhat larger (especially extending higher) than that seen in simulations of the NH December 1998 warming (Manney et al., 2000a). The strong tilt of the vortex with height during the warming led to low latitude air surrounding and overlying the vortices after they split, resulting in highly unusual trace gas profile structure.

Simulations driven with the NCEP/CPC and ECMWF analyses reproduced wave 2 major warmings, but those driven with GEOS data did not. The strong upward EP fluxes from wave 2 and higher wavenumbers at the boundary in the GEOS data decayed earlier than in the other analyses. Stronger latitudinal gradients at high latitudes in the GEOS 100 hPa geopotential heights than in the other analyses were shown to be the primary reason for the poorer GEOS-driven simulations.

Sensitivity tests with altered boundary fields with limited wavenumbers, varying wave amplitudes, varying wave 2 phase, constant forcing, and forcing that was constant after a given date, indicate a very strong dependence of the warming on the details of the boundary forcing. In contrast to some NH results (Butchart et al., 1982), wave 3 was needed in addition to wave 2 and the zonal mean in the boundary to produce a major warming. Simulations with stationary and phase-shifted wave 2 in the boundary produced major warmings, but of substantially different character than the observed event. The simulation of a major warming at this time thus depends critically on the lower boundary forcing, especially on the amplitude and upward propagation of wave 2.

Simulations with successively earlier initialization dates produced increasingly weaker warmings. In contrast, most simulations with altered initial states based on the 14 September 2002 fields produced major warmings similar to that observed. Simulations with initialization fields from 14 September in other years also produced major, or nearly major, warmings. The location and shape of the poleward edge of the region where wave 2 can propagate through the middle and upper stratosphere strongly affects the strength of the modeled warmings, with major warmings simulated for initial states where that boundary was at lower latitudes on 14 September; this allowed propagation such that deceleration occurred above the jet core in the initial stages of the warming. The 3D view of this effect shows wave-breaking and vortex erosion occurring first at upper levels in the cases with strongest warmings.

The overall results of the sensitivity tests show strong dependence on many small changes, suggesting that a very particular set of conditions were fulfilled allowing this major warming to occur. The extremely strong dependence on the boundary forcing indicates that it is, indeed, fair to view the extraordinary wave event in mid-September as the trigger and direct cause of the major warming. The flow regime in the SH in September 2002 may be similar to the “strong” flow regime seen in idealized experiments (Scaife and James, 2000; Gray et al., 2003) during which the occurrence of major warmings is controlled primarily by the boundary forcing. However, there is also sensitivity to the initial state, and, in any case, the unusual stratospheric flow immediately before the warming and the unusual 100 hPa forcing cannot be regarded as being independent (e.g., Charlton et al., this issue; Scaife et al., this issue). Scaife et al. show results indicating that the anomalous forcing in the lower stratosphere (e.g., at 100 hPa) develops from a less extraordinary wave pulse in the upper troposphere; future studies with the USMM boundary lowered to, e.g., 250 hPa, may thus be instructive to examine the model response to the tropospheric forcing underlying the huge wave pulse at 100 hPa. Other papers in this issue (e.g., Charlton et al.; Kushner and Polvani; Newman and Nash; Scaife et al.) explore some of the possible origins of the anomalous wave event that triggered the warming and the unusual conditions in the SH stratosphere leading up to this event.

**Acknowledgments.** Thanks to the UK Met Office and the British Atmospheric Data Centre for Met Office data, the GSFC ACD Science Data System (Eric Nash and Paul Newman) for NCEP/CPC Data, the German Weather Service (DWD) for ECMWF data, NASA’s Global Modeling and Assimilation Office

for GEOS-3 and GEOS-4 data, and the JPL Microwave Limb Sounder Team for technical assistance, data management and computer support. Thanks to Loïis Steenman-Clark for technical assistance with the USMM, Paul Newman for original routines used to calculate PV, Kirstin Krüger, Alan O'Neill, and the participants in the Royal Meteorological Society Atmospheric Chemistry Special Interest Group's special meeting on the SH 2002 winter for useful and stimulating discussions, and two anonymous reviewers for their helpful comments. The supercomputer used in this investigation was provided by the Jet Propulsion Laboratory, California Institute of Technology (JPL/CalTech) supercomputing project, which is funded by the NASA Offices of Earth Sciences, Aeronautics and Space Science. Work at JPL/CalTech was done under contract with the National Aeronautics and Space Administration. Work at the Data Assimilation Research Centre (DARC) was funded by the UK Natural Environment Research Council (NERC).

## References

- Allen, D. R., R. M. Bevilacqua, G. E. Nedoluha, C. E. Randall, and G. L. Manney, 2003: Unusual stratospheric transport and mixing during the 2002 Antarctic winter. *Geophys. Res. Lett.*, **30**, 1599, doi:10.1029/2003GL017117.
- Andrews, D. G., J. R. Holton, and C. B. Leovy, 1987: *Middle Atmosphere Dynamics*. Academic Press, San Diego, Calif., 1st ed.
- Baldwin, M. P., T. Hirooka, A. O'Neill, and S. Yoden, 2003: Major stratospheric warming in the southern hemisphere in 2002: Dynamical aspects of the ozone hole split. *SPARC Newsletter*, **No. 20**, 24–26.
- Butchart, N., S. A. Clough, T. N. Palmer, and P. J. Trevelyan, 1982: Simulations of an observed stratospheric warming with quasigeostrophic refractive index as a model diagnostic. *Q. J. R. Meteorol. Soc.*, **108**, 475–502.
- Charlton, A. J., A. O'Neill, W. A. Lahoz, P. Berrisford, P. van Velthoven, H. Eskes, and H. Kelder, 2004: The splitting of the stratospheric polar vortex in the southern hemisphere, september 2002: Dynamical evolution and impacts on ozone, *J. Atmos. Sci.*, *submitted*, 2004.
- Cohn, S. E., A. da Silva, J. Guo, M. Siekenwicz, and D. Lamich, 1998: Assessing the effects of data selection with the DAO physical-space statistical analysis system. *Mon. Weather Rev.*, **126**, 2913–2926.
- Douglass, A. R., M. R. Schoeberl, R. B. Rood, and S. Pawson, 2003: Evaluation of transport in the lower tropical stratosphere in a global chemistry and transport model. *J. Geophys. Res.*, **108**, 4259, doi:10.1029/2002JD002696.
- Dunkerton, T. J. and D. P. Delisi, 1986: Evolution of potential vorticity in the winter stratosphere of January-February 1979. *J. Geophys. Res.*, **91**, 1199–1208.
- Fairlie, T. D. A., M. Fisher, and A. O'Neill, 1990a: The development of narrow baroclinic zones and other small-scale structure in the stratosphere during simulated major warmings. *Q. J. R. Meteorol. Soc.*, **116**, 287–315.
- Fairlie, T. D. A. and A. O'Neill, 1988: The stratospheric major warming of winter 1984/1985: observations and dynamical inferences. *Q. J. R. Meteorol. Soc.*, **114**, 557–578.
- Fairlie, T. D. A., A. O'Neill, and V. D. Pope, 1990b: The sudden breakdown of an unusually strong cyclone in the stratosphere during winter 1988/89. *Q. J. R. Meteorol. Soc.*, **116**, 767–774.

- Gray, L. J., W. Norton, C. Pascoe, and A. Charlton, 2004: A possible influence of equatorial winds on the September 2002 southern hemisphere sudden warming event, *J. Atmos. Sci.*, *submitted*, 2004.
- Gray, L. J., S. Sparrow, M. Jukes, A. O'Neill, and D. G. Andrews, 2003: Flow regimes in the winter stratosphere of the northern hemisphere. *Q. J. R. Meteorol. Soc.*, **129**, 925–945.
- Hoppel, K. W., R. Bevilacqua, G. Nedoluha, C. Deniel, F. Lefevre, J. Lumpe, M. Fromm, C. Randall, J. Rosenfield, and M. Rex, 2003: POAM III observations of the anomalous 2002 Antarctic ozone hole. *Geophys. Res. Lett.*, **30**, doi:10.1029/2003GL016899.
- Jung, J.-H., C. S. Konor, C. R. Mechoso, and A. Arakawa, 2001: A study of the stratospheric major warming and subsequent flow recovery during the winter of 1979 with an isentropic vertical coordinate model. *J. Atmos. Sci.*, **58**, 2630–2649.
- Kanzawa, H., 1980: The behavior of mean zonal wind and planetary-scale disturbances in the troposphere and stratosphere during the 1973 sudden warming. *J. Meteorol. Soc. Jap.*, **58**, 329–356.
- Kondragunta, S. et al., 2004: Vertical structure of the anomalous 2002 Antarctic ozone hole, *J. Atmos. Sci.*, *submitted*, 2004.
- Krüger, K., B. Naujokat, and K. Labitzke, 2004: The unusual midwinter warming in the southern hemisphere stratosphere 2002: A comparison to northern hemisphere phenomena, *J. Atmos. Sci.*, *accepted*, 2004.
- Kushner, P. J. and L. M. Polvani, 2004: A very large, spontaneous stratospheric sudden warming in a simple AGCM: A prototype for the southern-hemisphere warming of 2002?, *J. Atmos. Sci.*, *submitted*, 2004.
- Labitzke, K., 1977: Interannual variability of the winter stratosphere in the Northern Hemisphere. *Mon. Weather Rev.*, **105**, 762–770.
- , 1982: On the interannual variability of the middle stratosphere during the Northern winters. *J. Met. Soc. Japan*, **60**, 124–139.
- Lin, S.-J., 2004: A vertically Lagrangian finite-volume dynamical core for global models, *Mon. Wea. Rev.*, *submitted*, 2004.
- MacKenzie, I. A., R. S. Harwood, P. A. Stott, and G. C. Watson, 1999: Radiative-dynamic effects of the Antarctic ozone hole and chemical feedback. *Q. J. R. Meteorol. Soc.*, **125**, 2171–2203.
- Manney, G. L., R. M. Bevilacqua, K. W. Hoppel, W. A. Lahoz, A. O'Neill, and J. M. Russell III, 2000a: Observations and modeling of transport during the December 1998 stratospheric major warming. In

- Amer. Meteorol. Soc. 11th Conference on the Middle Atmosphere*, Long Beach, CA, 9–14 January 2000.
- Manney, G. L., J. D. Farrara, and C. R. Mechoso, 1994a: Simulations of the February 1979 stratospheric sudden warming: Model comparisons and three-dimensional evolution. *Mon. Weather Rev.*, **122**, 1115–1140.
- Manney, G. L., W. A. Lahoz, J. L. Sabutis, A. O’Neill, and L. Steenman-Clark, 2002: Simulations of fall and early winter in the stratosphere. *Q. J. R. Meteorol. Soc.*, **128**, 2205–2237.
- Manney, G. L., W. A. Lahoz, R. Swinbank, A. O’Neill, P. M. Connew, and R. W. Zurek, 1999: Simulation of the December 1998 stratospheric major warming. *Geophys. Res. Lett.*, **26**, 2733–2736.
- Manney, G. L., H. A. Michelsen, F. W. Irion, M. R. Gunson, G. C. Toon, and A. E. Roche, 2000b: Lamination and polar vortex development in fall from ATMOS long-lived trace gases observed during November 1994. *J. Geophys. Res.*, **105**, 29,023–29,038.
- Manney, G. L., J. L. Sabutis, S. Pawson, M. L. Santee, B. Naujokat, R. Swinbank, M. E. Gelman, and W. Ebisuzaki, 2003: Lower stratospheric temperature differences between meteorological analyses in two cold Arctic winters and their impact on polar processing studies. *J. Geophys. Res.*, **108**, 8328, doi:10.1029/2001JD001149.
- Manney, G. L., R. Swinbank, S. T. Massie, M. E. Gelman, A. J. Miller, R. Nagatani, A. O’Neill, and R. W. Zurek, 1996: Comparison of U. K. Meteorological Office and U. S. National Meteorological Center stratospheric analyses during northern and southern winter. *J. Geophys. Res.*, **101**, 10,311–10,334.
- Manney, G. L., R. W. Zurek, A. O’Neill, and R. Swinbank, 1994b: On the motion of air through the stratospheric polar vortex. *J. Atmos. Sci.*, **51**, 2973–2994.
- Matsuno, T., 1970: Vertical propagation of stationary waves in the winter northern hemisphere. *J. Atmos. Sci.*, **27**, 871–883.
- McIntyre, M. E. and T. N. Palmer, 1983: Breaking planetary waves in the stratosphere. *Nature*, **305**, 593–600.
- Naujokat, B., K. Krüger, K. Matthes, J. Hoffmann, M. Kunze, and K. Labitzke, 2002: The early major warming in December 2001 – exceptional? *Geophys. Res. Lett.*, **29**, doi:10.1029/2002GL015316.
- Newman, P. A., L. R. Lait, M. R. Schoeberl, R. M. Nagatani, and A. J. Krueger, 1989: Meteorological atlas of the Northern Hemisphere lower stratosphere for January and February 1989 during the Airborne Arctic Stratospheric Expedition. Tech. Rep. 4145, NASA.

- Newman, P. A. and E. R. Nash, 2004: The unusual southern hemisphere stratosphere winter of 2002, *J. Atmos. Sci.*, *submitted*, 2004.
- O'Neill, A. and V. D. Pope, 1988: Simulations of linear and nonlinear disturbances in the stratosphere. *Q. J. R. Meteorol. Soc.*, **114**, 1063–1110.
- Plumb, R. A., 1985: On the three-dimensional propagation of stationary waves. *J. Atmos. Sci.*, **42**, 217–229.
- Polvani, L. M. and R. Saravanan, 2000: The three-dimensional structure of breaking Rossby waves in the polar wintertime stratosphere. *J. Atmos. Sci.*, **57**, 3663–3685.
- Randall, C. E., G. L. Manney, D. R. Allen, R. M. Bevilacqua, C. Trepte, W. A. Lahoz, and A. O'Neill, 2004: Reconstruction and simulation of stratospheric ozone distributions during the 2002 austral winter, *J. Atmos. Sci.*, *accepted*, 2004.
- Sabutis, J. L., 1997: The short-term transport of zonal mean ozone using a residual mean circulation calculated from observations. *J. Atmos. Sci.*, **54**, 1094–1106.
- Sabutis, J. L., R. P. Turco, and S. K. Kar, 1997: Wintertime planetary wave propagation in the lower stratosphere and its observed effect on northern hemisphere temperature-ozone correlations. *J. Geophys. Res.*, **102**, 21,709–21,717.
- Scaife, A. A. and I. N. James, 2000: Response of the stratosphere to interannual variability of tropospheric planetary waves. *Q. J. R. Meteorol. Soc.*, **126**, 275–297.
- Scaife, A. A., R. Swinbank, D. R. Jackson, N. Butchart, H. Thornton, M. Keil, and L. Henderson, 2004: Stratospheric vacillations and the major warming over Antarctica in 2002, *J. Atmos. Sci.*, *submitted*, 2004.
- Schoeberl, M. R., A. R. Douglass, Z. Zhu, and S. Pawson, 2003: A comparison of the lower stratospheric age spectra derived from a general circulation model and two data assimilation systems. *J. Geophys. Res.*, **108**, 4113, doi:10.1029/2002JD002652.
- Scott, R. K. and P. H. Haynes, 1998: Internal interannual variability of the extratropical stratospheric circulation: The low-latitude flywheel. *Q. J. R. Meteorol. Soc.*, **124**, 2149–2173.
- Shine, K. P., 1987: The middle atmosphere in the absence of dynamic heat fluxes. *Q. J. R. Meteorol. Soc.*, **113**, 603–633.
- Simmons, A. J., M. Hortal, G. Kelly, A. McNally, A. Untch, and S. Uppala, 2004: ECMWF analyses and forecasts of stratospheric winter polar vortex break-up: September 2002 in the southern hemisphere and related events, *J. Atmos. Sci.*, *accepted*, 2004.

- Sinnhuber, B.-M., M. Weber, A. Amankwah, and J. P. Burrows, 2003: Total ozone during the unusual Antarctic winter of 2002. *Geophys. Res. Lett.*, 1580 doi:10.1029/2002GL016798.
- Smith, A. K., 1992: Preconditioning for stratospheric sudden warmings: Sensitivity studies with a numerical model. *J. Atmos. Sci.*, **49**, 1003–1019.
- Swinbank, R., N. B. Ingleby, P. M. Boorman, and R. J. Renshaw, 2002: A 3D variational data assimilation system for the stratosphere and troposphere. Tech. Rep. 71, Met Office Numerical Weather Prediction Forecasting Research Scientific Paper.
- Swinbank, R. and A. O'Neill, 1994: A stratosphere-troposphere data assimilation system. *Mon. Weather Rev.*, **122**, 686–702.
- Thuburn, J. and R. Brugge, 1994: The UGAMP stratosphere mesosphere model. Tech. Rep. Internal Rep. No. 34, UGAMP.
- Varotsos, C., 2002: The southern hemisphere ozone hole split in 2002. *Environ. Sci. and Pollut. Res.*, **9**, 375–376.
- Weber, M., S. Dhomse, F. Wittrock, A. Richter, B. M. Sinnhuber, and J. P. Burrows, 2003: Dynamical control of NH and SH winter/spring total ozone from GOME observations in 1995-2002. *Geophys. Res. Lett.*, **30**, 1583, doi:10.1029/2002GL016799.
-

## Figure Captions

**Figure 1.** 100 hPa geopotential heights (km) on 20, 22, 24 and 26 September 2002 from Met Office analyses. Contour interval is 0.1 km, with 15.0–15.2 km darkly shaded and 16.3–16.8 km lightly shaded. Projection is orthographic, with 0°E at the top and 90°E at the right; the domain is 0–90°S with dotted lines at 30 and 60°S.

**Figure 2.** Time series of Met Office and USMM (top to bottom) 10 hPa zonal mean winds, zonal mean temperatures, and wave 1 and wave 2 geopotential heights. Wind contour interval is 5 m/s, with values less than zero shaded. Temperature contour interval is 2.5 K, with 215–225 K darkly shaded and values over 240 K lightly shaded. Wave 1 contour interval is 200 m, with 800–1000 m shaded. Wave 2 contour interval is 100 m, with 400 to 500 m shaded. Dots in wave 1 and wave 2 plots indicate the phase (longitude of one maximum) at 60°S.

**Figure 3.** Time series of Met Office and USMM 60°S (top to bottom) zonal mean winds, zonal mean temperatures, and wave 1 and wave 2 geopotential heights. Wind contour interval is 10 m/s, with values less than zero shaded. Temperature contour interval is 3.0 K, with 216–225 K lightly shaded and 234–240 K darkly shaded. Wave 1 contour interval is 150 m, with 600–750 m shaded. Wave 2 contour interval is 100 m, with 500 to 600 m shaded.

**Figure 4.** Met Office and USMM 840 K sPV ( $10^{-4} \text{ s}^{-1}$ , colors) maps on 22, 25, 28 September and 1 October 2002. Temperatures at 10 K intervals from 200 to 260 K are overlaid in white. Layout is as in Figure 1.

**Figure 5.** Isosurfaces of the  $1.6 \times 10^{-4} \text{ s}^{-1}$  contour (in the vortex edge region) of sPV from Met Office analyses and USMM, on 26, 28 September and 6 October 2002. Vertical range in 450–1600 K.

**Figure 6.** Vertical velocities (cm/s, colors) and Temperatures (K, contours) around the 60°S latitude circle on 25 September 2002. Temperature contour interval is 5 K, with blue contours at and below 235 K, black contours above. Thin vertical line is at 180°E

**Figure 7.** EP flux vectors (arrows) and divergences (m/s/d, colors, negative values represent deceleration of the zonal wind) from the Met Office analyses and the USMM simulation, on 22 and 26 September 2002.

**Figure 8.** 3D EP fluxes (arrows show horizontal components, colors vertical component) from the Met Office and USMM on 22 and 26 September 2002, at 10 and 46 hPa. Two sPV contours on a comparable isentropic surface (840 K for 10 hPa, 465 K for 46 hPa) representative of the vortex edge are overlaid in white. Low temperature contours are overlaid in blue (5 K interval, 200 to 225 at 10 hPa and 180 to 205 at 46 hPa) and high temperature contours in black (5 K interval, 230 to 240 K at 10 hPa and 210 to 220 K at 46 hPa). Projection is orthographic, with 0°E at the top and 90°E at the right; the domain is 0-90°S with dotted lines at 30 and 60°S.

**Figure 9.** Cross-sections around 60°S of USMM CH<sub>4</sub> and EqL-tracer (see text) from the control simulation on 26 and 28 September 2002. Overlaid contours are sPV in the vortex edge region (-1.2, -1.8 and  $-2.4 \times 10^{-4} \text{ s}^{-1}$ ). Thin vertical line is at 180°E.

**Figure 10.** USMM CH<sub>4</sub> (ppmv) on 14 September 2002 and 6 October 2002, and the difference between them (6 October – 14 September, so decreases are negative). Horizontal axis is EqL.

**Figure 11.** 10-hPa zonal mean winds (m/s) from (top to bottom) ECMWF, NCEP/CPC, GEOS-3 and GEOS-4 analyses (left) and USMM simulations driven with those analyses (right). Contour interval is 5 m/s, with negative values shaded.

**Figure 12.** 840-K sPV maps on 25 and 28 September 2002 from GEOS-4 driven USMM simulation. Layout and contouring are as in Figure 4.

**Figure 13.** 10-hPa zonal mean winds (m/s) and wave 1 and 2 geopotential heights from USMM runs with waves 1 and 2 only in the boundary field (left), waves 1–3 in the boundary field (center), and waves 2 and 3 only in the boundary field (right). Contouring is as in Figure 2. Dots in wave 1 and wave 2 plots indicate the phase (longitude of one maximum) at 60°S.

**Figure 14.** 10-hPa zonal mean winds (m/s) from USMM runs with fixed wave 2 phase in the boundary and 90° phase-shifted wave 2 in boundary. Contouring is as in Figure 2.

**Figure 15.** 840-K sPV maps on 28 September for the runs with fixed wave 2 phase in the boundary and 90° phase-shifted wave 2 in boundary. Layout and contouring are as in Figure 4.

**Figure 16.** Initial zonal mean wind fields for 14 September 2002, 14 September 1997, 14 September 2001, and 14 September 2002 zonal mean winds from a USMM run initialized on 27 July 2002. Contour interval is 5 m/s, with dashed contours for negative values. The shaded regions show areas with negative index of refraction for wave 2.

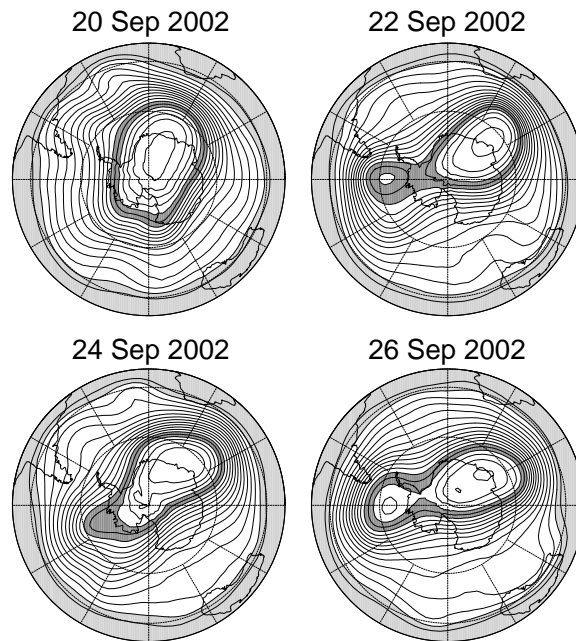
**Figure 17.** 10-hPa zonal mean winds (m/s) from USMM runs with zonal mean only 14 September 2002 initial fields, 14 September 1997 initial fields, and 14 September 2001 initial fields. Contouring is as in Figure 2.

**Figure 18.** 840-K sPV maps on 26 September from run with 14 September 1997 initial field, and 28 September from run with 14 September 2001 initial field. Layout and contouring are as in Figure 4.

## Tables

**Table 1.** USMM sensitivity tests to different initial and boundary conditions. Upper box shows tests of sensitivity to boundary forcing, lower box to initial conditions.

Init Date	Initial Field	Boundary Field	Results
14 Sep 2002	MetO data	zonal mean + waves 1–2	strong warming
14 Sep 2002	MetO data	zonal mean + waves 1–3	major warming
14 Sep 2002	MetO data	zonal mean + waves 2–3	major warming
14 Sep 2002	MetO data	wave 2 stationary	major wave 1,2 warming
14 Sep 2002	MetO data	wave 2 shifted 90°	major wave 1,2 warming
14 Sep 2002	MetO data	0.5×wave 1–6 amps	no significant warming
14 Sep 2002	MetO data	0.75×wave 1–6 amps	minor warming
14 Sep 2002	MetO data	const field, avg 30 days before init	no warming
14 Sep 2002	MetO data	constant field, 22 Sep zonal mean + 0.6×wave 1-6 amps	minor warming
14 Sep 2002	MetO data	MetO data through 22 Sep, const. thereafter at 22 Sep value	later major wave 1 warming
11 Sep 2002	MetO data	MetO data	strong wave 2 warming
17 Sep 2002	MetO data	MetO data	weaker major wave 2 warm- ing
Earlier Inits	MetO data	MetO data	strong wave 2 warming
14 Sep 2002	1.1×zonal mean winds	MetO data	major wave 2 warming
14 Sep 2002	1.25×zonal mean winds	MetO data	major wave 2 warming
14 Sep 2002	Zonal mean only	MetO data	major wave 2 warming
14 Sep 1997	MetO data	Sep-Oct 2002 MetO data	strong wave 2 warming
14 Sep 2001	MetO data	Sep-Oct 2002 MetO data	major wave 2 warming

**Figures**

**Figure 1.** 100 hPa geopotential heights (km) on 20, 22, 24 and 26 September 2002 from Met Office analyses. Contour interval is 0.1 km, with 15.0–15.2 km darkly shaded and 16.3–16.8 km lightly shaded. Projection is orthographic, with 0°E at the top and 90°E at the right; the domain is 0–90°S with dotted lines at 30 and 60°S.

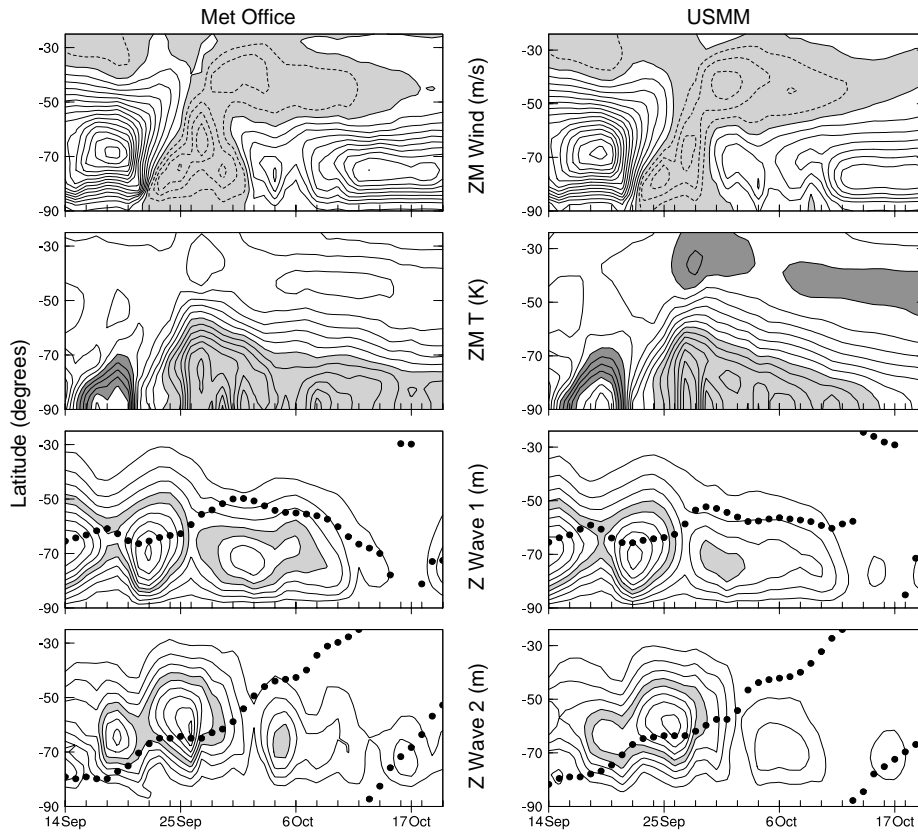


**Figure 2.** Time series of Met Office and USMM (top to bottom) 10 hPa zonal mean winds, zonal mean temperatures, and wave 1 and wave 2 geopotential heights. Wind contour interval is 5 m/s, with values less than zero shaded. Temperature contour interval is 2.5 K, with 215–225 K darkly shaded and values over 240 K lightly shaded. Wave 1 contour interval is 200 m, with 800–1000 m shaded. Wave 2 contour interval is 100 m, with 400 to 500 m shaded. Dots in wave 1 and wave 2 plots indicate the phase (longitude of one maximum) at 60°S.

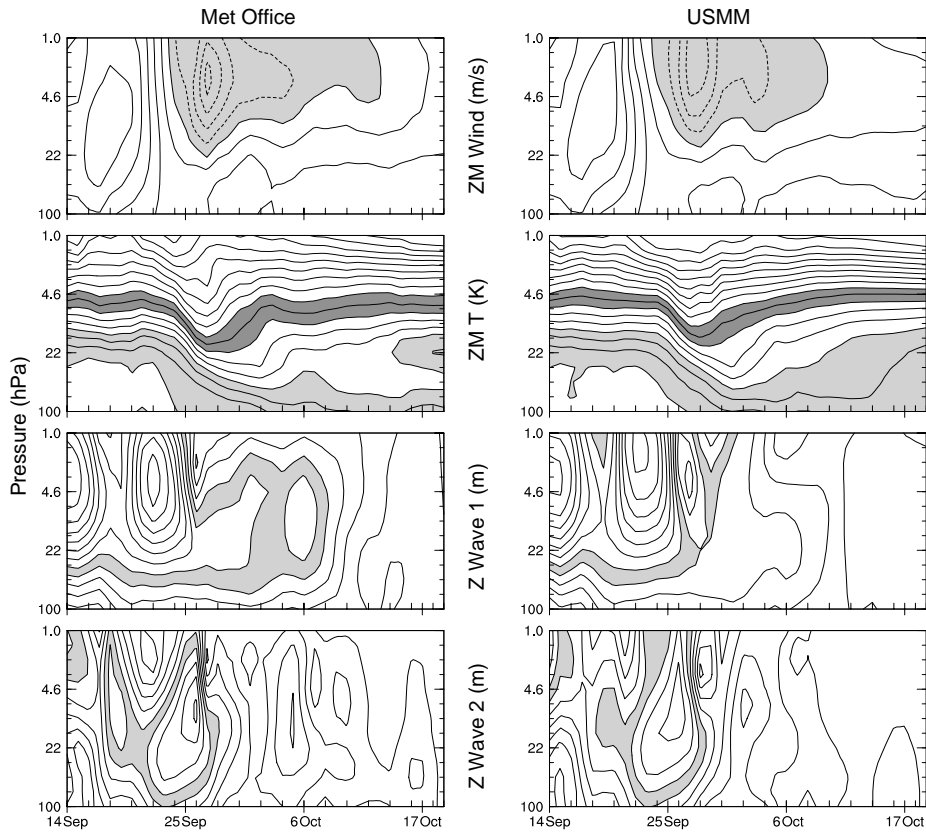


**Figure 3.** Time series of Met Office and USMM 60°S (top to bottom) zonal mean winds, zonal mean temperatures, and wave 1 and wave 2 geopotential heights. Wind contour interval is 10 m/s, with values less than zero shaded. Temperature contour interval is 3.0 K, with 216–225 K lightly shaded and 234–240 K darkly shaded. Wave 1 contour interval is 150 m, with 600–750 m shaded. Wave 2 contour interval is 100 m, with 500 to 600 m shaded.

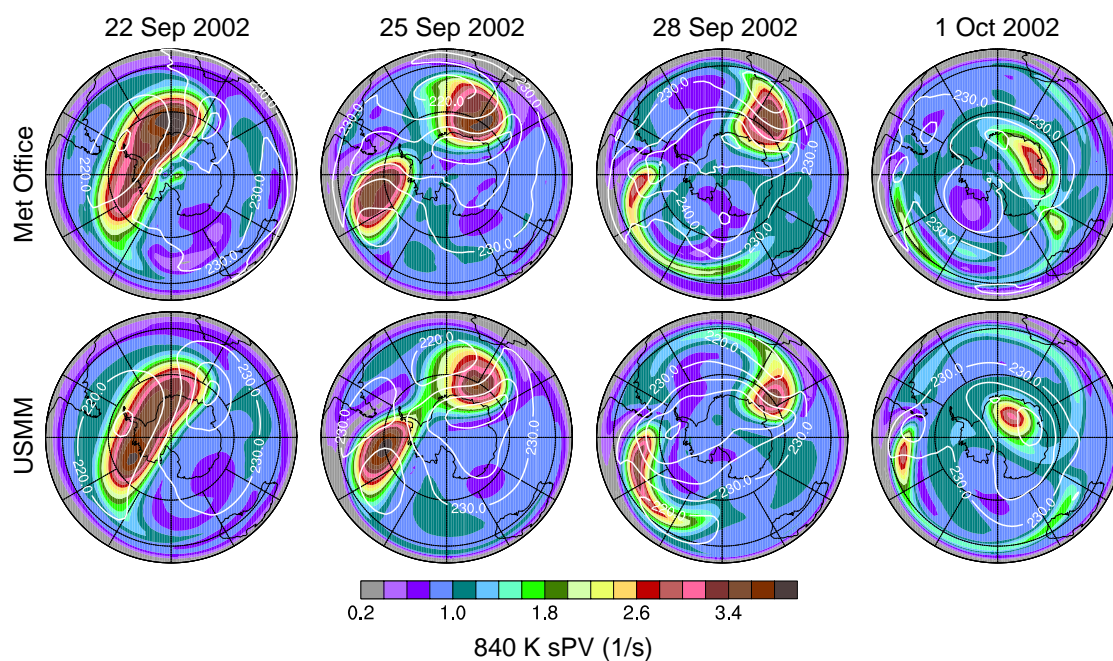


**Figure 4.** Met Office and USMM 840 K sPV ( $10^{-4} \text{ s}^{-1}$ , colors) maps on 22, 25, 28 September and 1 October 2002. Temperatures at 10 K intervals from 200 to 260 K are overlaid in white. Layout is as in Figure 1.

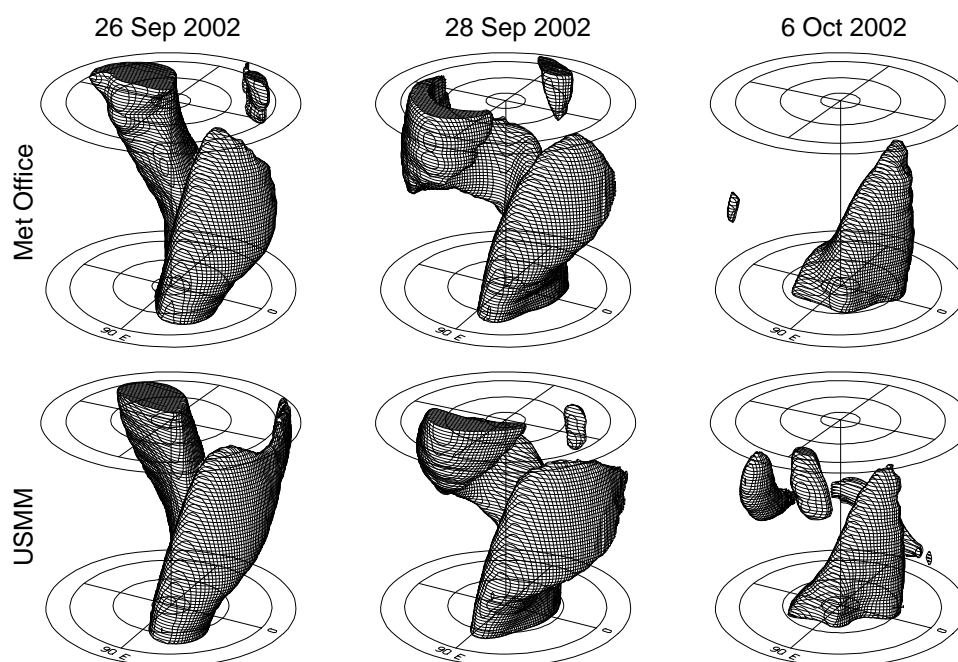


**Figure 5.** Isosurfaces of the  $1.6 \times 10^{-4} \text{ s}^{-1}$  contour (in the vortex edge region) of sPV from Met Office analyses and USMM, on 26, 28 September and 6 October 2002. Vertical range in 450–1600 K.

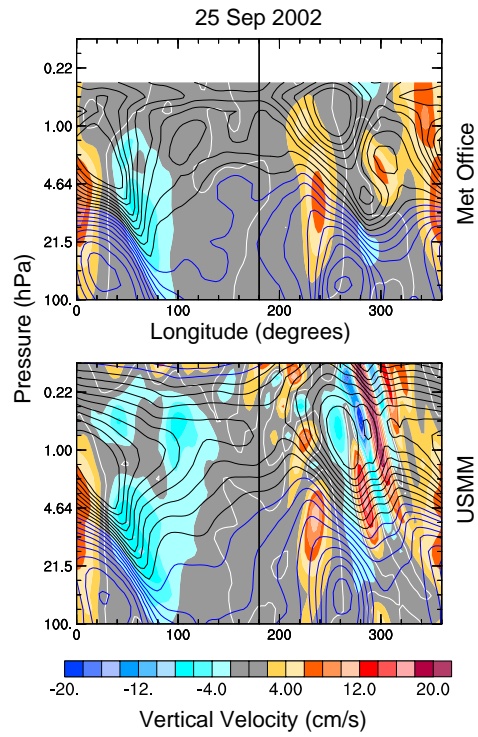


**Figure 6.** Vertical velocities (cm/s, colors) and Temperatures (K, contours) around the  $60^{\circ}\text{S}$  latitude circle on 25 September 2002. Temperature contour interval is 5 K, with blue contours at and below 235 K, black contours above. Thin vertical line is at  $180^{\circ}\text{E}$

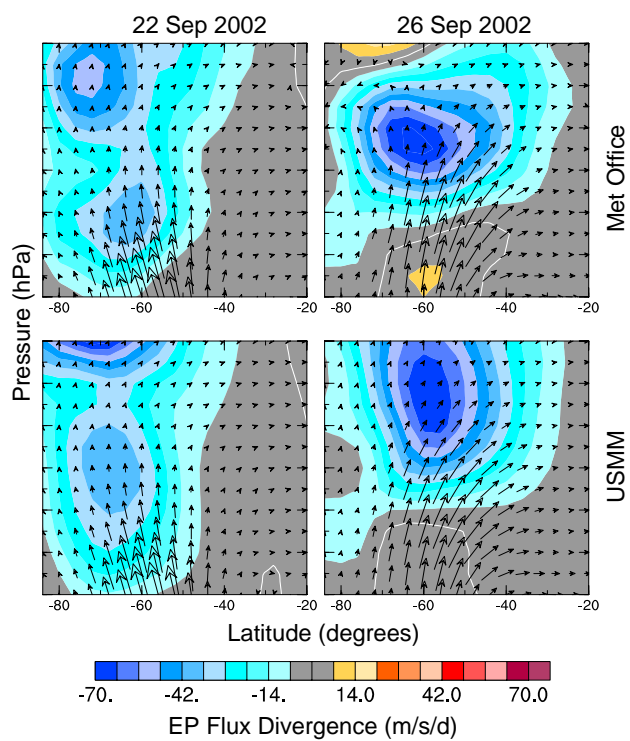


**Figure 7.** EP flux vectors (arrows) and divergences (m/s/d, colors, negative values represent deceleration of the zonal wind) from the Met Office analyses and the USMM simulation, on 22 and 26 September 2002.

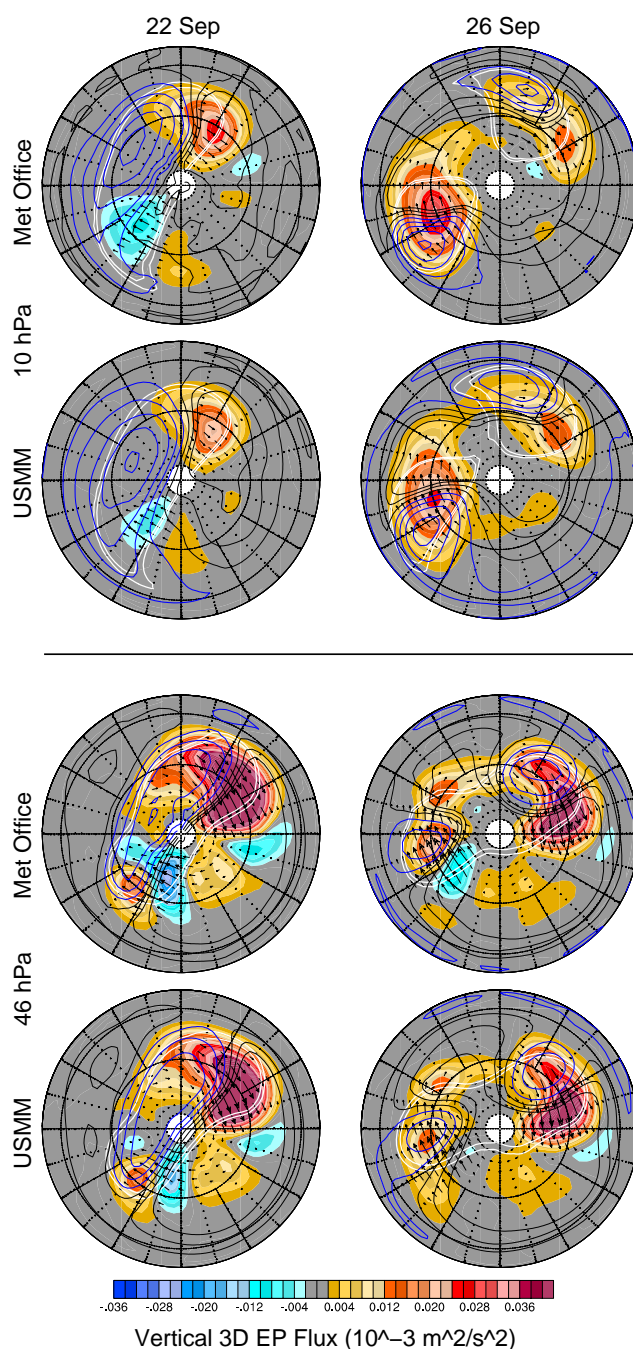


**Figure 8.** 3D EP fluxes (arrows show horizontal components, colors vertical component) from the Met Office and USMM on 22 and 26 September 2002, at 10 and 46 hPa. Two sPV contours on a comparable isentropic surface (840 K for 10 hPa, 465 K for 46 hPa) representative of the vortex edge are overlaid in white. Low temperature contours are overlaid in blue (5 K interval, 200 to 225 at 10 hPa and 180 to 205 at 46 hPa) and high temperature contours in black (5 K interval, 230 to 240 K at 10 hPa and 210 to 220 K at 46 hPa). Projection is orthographic, with 0°E at the top and 90°E at the right; the domain is 0-90°S with dotted lines at 30 and 60°S.

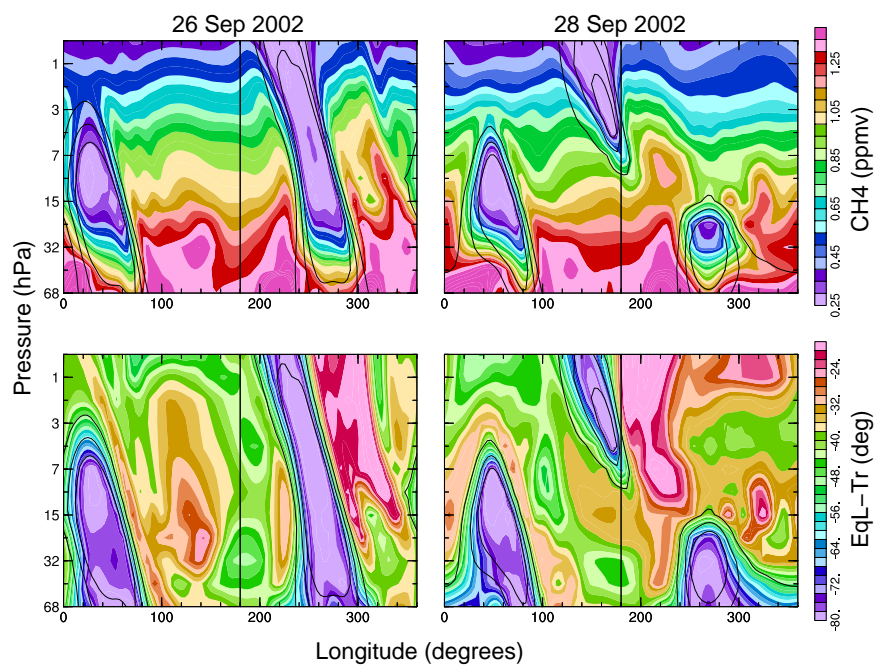


**Figure 9.** Cross-sections around  $60^{\circ}\text{S}$  of USMM  $\text{CH}_4$  and EqL-tracer (see text) from the control simulation on 26 and 28 September 2002. Overlaid contours are sPV in the vortex edge region ( $-1.2, -1.8$  and  $-2.4 \times 10^{-4} \text{ s}^{-1}$ ). Thin vertical line is at  $180^{\circ}\text{E}$ .

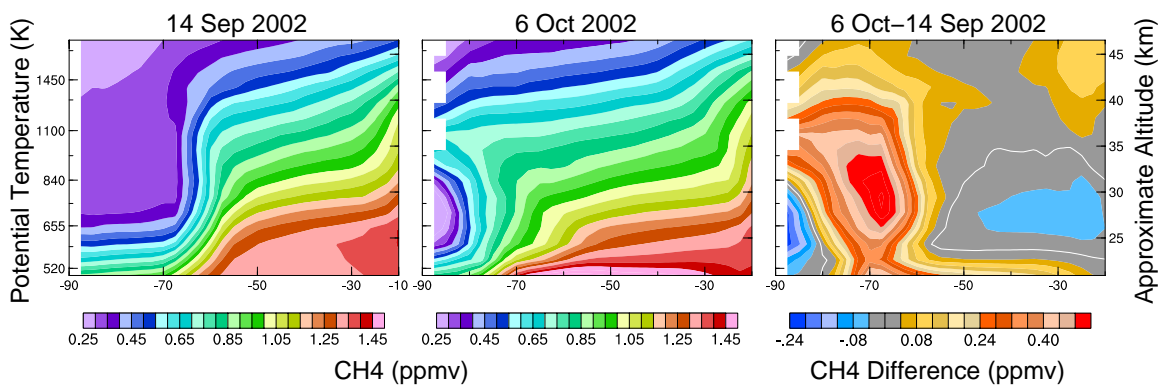


**Figure 10.** USMM  $\text{CH}_4$  (ppmv) on 14 September 2002 and 6 October 2002, and the difference between them (6 October – 14 September, so decreases are negative). Horizontal axis is EqL.

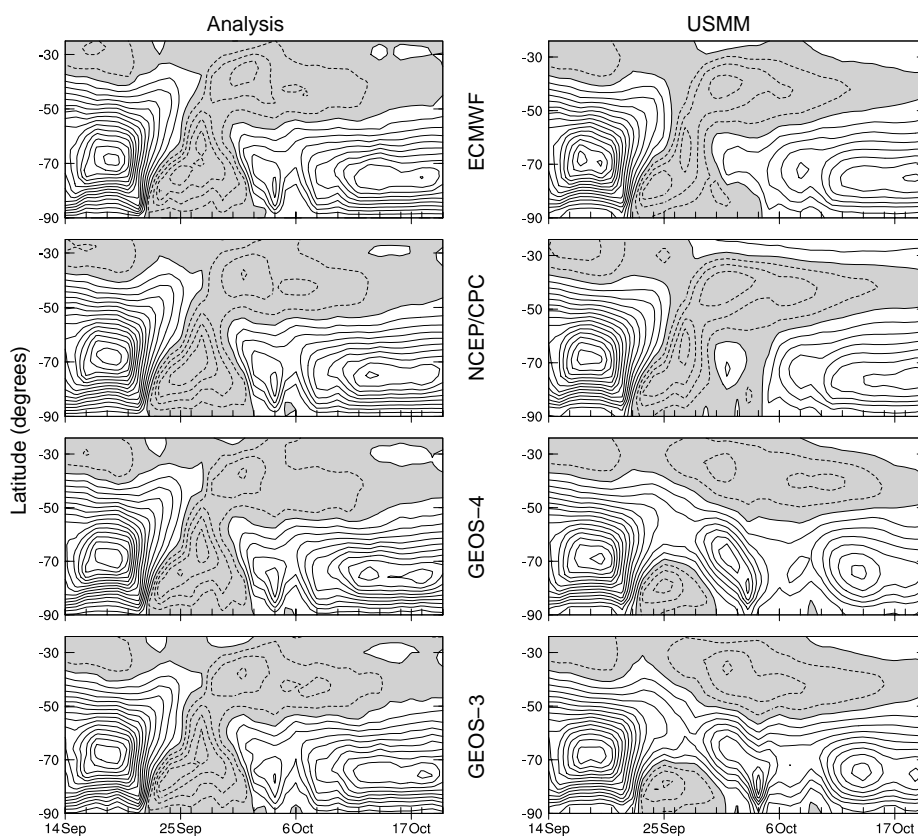


**Figure 11.** 10-hPa zonal mean winds (m/s) from (top to bottom) ECMWF, NCEP/CPC, GEOS-3 and GEOS-4 analyses (left) and USMM simulations driven with those analyses (right). Contour interval is 5 m/s, with negative values shaded.

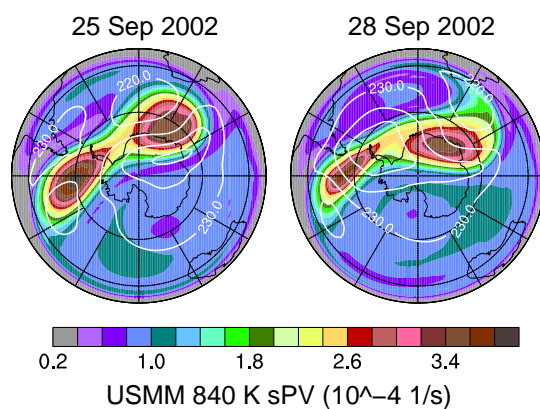


**Figure 12.** 840-K sPV maps on 25 and 28 September 2002 from GEOS-4 driven USMM simulation. Layout and contouring are as in Figure 4.

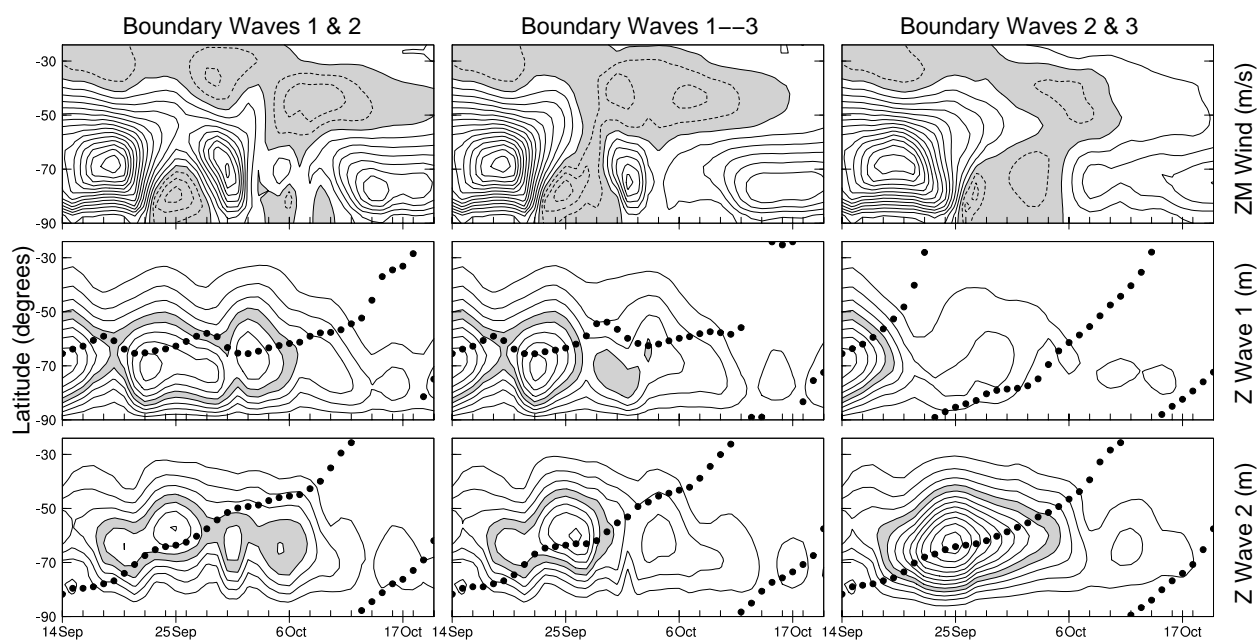


**Figure 13.** 10-hPa zonal mean winds (m/s) and wave 1 and 2 geopotential heights from USMM runs with waves 1 and 2 only in the boundary field (left), waves 1–3 in the boundary field (center), and waves 2 and 3 only in the boundary field (right). Contouring is as in Figure 2. Dots in wave 1 and wave 2 plots indicate the phase (longitude of one maximum) at  $60^{\circ}\text{S}$ .

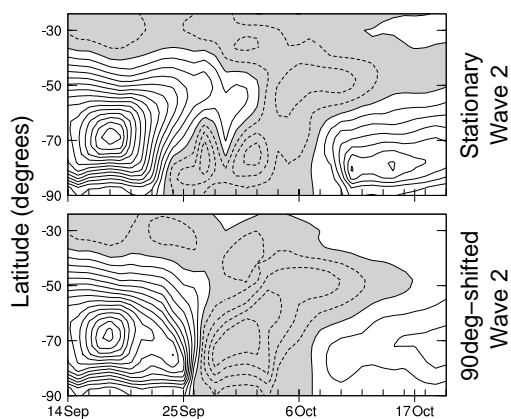


**Figure 14.** 10-hPa zonal mean winds (m/s) from USMM runs with fixed wave 2 phase in the boundary and  $90^{\circ}$  phase-shifted wave 2 in boundary. Contouring is as in Figure 2.

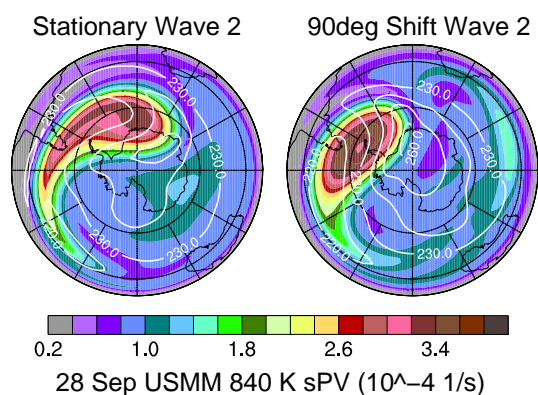


**Figure 15.** 840-K sPV maps on 28 September for the runs with fixed wave 2 phase in the boundary and  $90^\circ$  phase-shifted wave 2 in boundary. Layout and contouring are as in Figure 4.

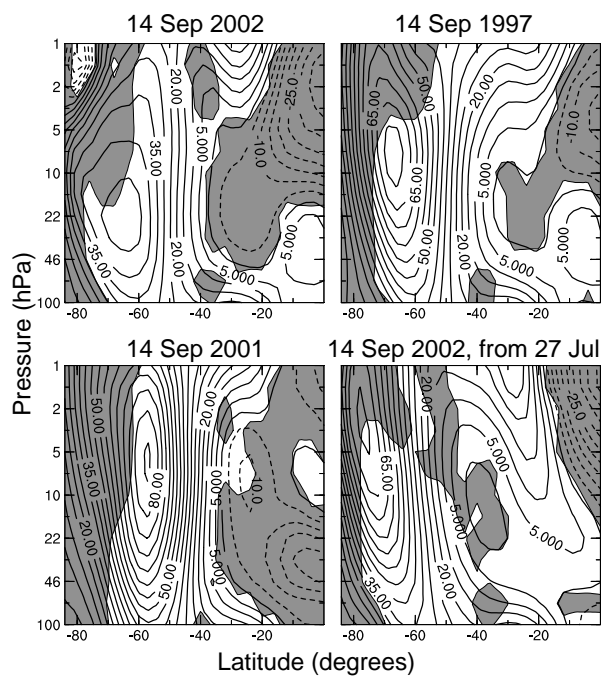


**Figure 16.** Initial zonal mean wind fields for 14 September 2002, 14 September 1997, 14 September 2001, and 14 September 2002 zonal mean winds from a USMM run initialized on 27 July 2002. Contour interval is 5 m/s, with dashed contours for negative values. The shaded regions show areas with negative index of refraction for wave 2.

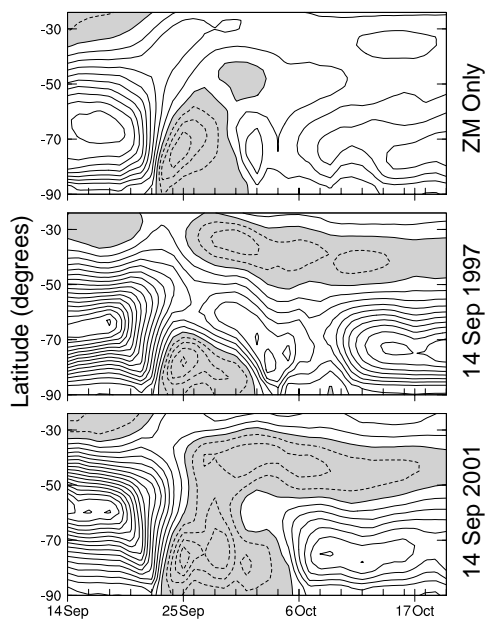


**Figure 17.** 10-hPa zonal mean winds (m/s) from USMM runs with zonal mean only 14 September 2002 initial fields, 14 September 1997 initial fields, and 14 September 2001 initial fields. Contouring is as in Figure 2.

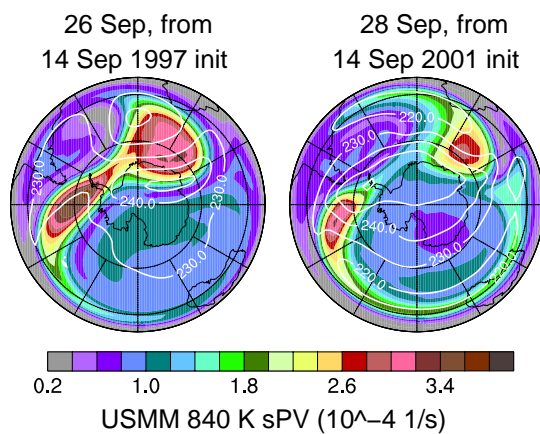


**Figure 18.** 840-K sPV maps on 26 September from run with 14 September 1997 initial field, and 28 September from run with 14 September 2001 initial field. Layout and contouring are as in Figure 4.